CHAPTER 12

Semiconductor Nanowire Lasers

C. Z. Ning

Contents

School of Electrical, Computer, and Energy Engineering, Arizona State University, Tempe, AZ, USA

Semiconductors and Semimetals, Volume 86
ISSN 0080-8784, DOI: 10.1016/B978-0-12-391066-0.00012-5

1. INTRODUCTION

Semiconductor nanowires (NWs) are quasi-one-dimensional structures with diameters typically in the range of 10s–100s of nanometers and lengths in the range from a few to hundreds of microns. They are very often large enough such that quantum-size effects can be ignored and thus not quantum wires. But optically, they are high-quality one-dimensional waveguides with cross-sections in rectangular, triangular, hexagonal, or cylindrical forms. There is usually a high contrast between the refractive indices of the wires, in the range of 2.5–3.5, and the surroundings, typically air. Such high contrast makes wires as small as a few hundred nanometers very good optical waveguides. Nanowires are also potentially very efficient optoelectronic structures either as waveguides or as laser cavities, since there is a large overlap of optical and electronic modes, as described by the optical modal confinement factors (Maslov and Ning, 2004b). Individual nanowires can work as laser cavities, making them among the smallest of any semiconductor lasers.

This chapter focuses on the major developments of the past 10 years in the area of semiconductor nanowire lasers and related optical studies. Semiconductor nanowire lasers represent a unique development in the history of semiconductor lasers. The major developments of the past 10 years are largely not from the traditional optoelectronics, or semiconductor laser community; the pioneering initial contributions were made by researchers from chemistry and materials communities. Ten years after the initial demonstration of nanowire lasing (Huang *et al.*, 2001), the larger optoelectronic community is beginning to appreciate the usefulness and importance of such unique nanostructures, as evidenced by the recent special issue of *IEEE Selected Topics in Quantum Electronics*, see Jagadish *et al.* (2011). As the materials quality improves and more suited device structures are fabricated, especially using fabrication technologies that are more compatible with the standard III–V device fabrication, nanowire technology is bound to attract more attention from the optoelectronics community. Part of the purpose of this chapter is to introduce the nanowire lasers to the wider optoelectronics community so that more device physicists and engineers can be involved in the development of this unique technology. Interested readers can also consult many other review papers from various perspectives that focus on the optical and laser applications of semiconductor nanowires (Ning, 2010; Pan *et al.*, 2011; Vanmaekelbergh and van Vugt, 2011; Yan *et al.*, 2009; Yang, 2002; Zimmler *et al.*, 2010).

2. GROWTH OF SEMICONDUCTOR NANOWIRES

The most prevailing methods of growing quasi-one-dimensional NWs are based on the now well-known vapor–liquid–solid (VLS) mechanism. The VLS mechanism was established almost 50 years ago by Wagner and Ellis (1964) in the growth of Si whiskers of micron sizes. This directional growth of single crystal relies on the initial existence of a catalyst, very often metallic particles such as Au. Either Au film is deposited or Au nanoparticles are dispersed on the initial substrate. The adsorption of vapor phase semiconductor into the metal particles significantly lowers the melting point of semiconductor–metal alloy, such that the liquid alloy droplets are formed at a moderately elevated temperature on a substrate. With the continuous provision of semiconductor in vapor phase, the continuous adsorption on to the liquid droplets leads to supersaturation of alloy droplets. The resulting precipitation or nucleation leads to the initial growth of solid wires along a preferential crystal direction, leaving the liquid alloy droplets largely intact. One of the great advantages of such growth is that it allows defect-free growth, since the size of such quasi-one-dimensional objects (wires, rods, belts, ribbons, or whiskers) is typically smaller than the critical dimension of defect formation under a wide range of growth conditions. Such VLS mechanism was also observed in naturally occurring process such as germanium sulfide whiskers formed around the gas vents of burning anthracite coal (Finkelman *et al.*, 1974), where whiskers of 5μm in diameter and 100μm in length were observed. The VLS technique demonstrated by Wagner and Ellis (1964; Wu and Yang, 2001) received otherwise not much attention until almost 30 years later, when Hiruma and others at Hitachi studied the growth of InAs and GaAs nanowhiskers (Haraguchi *et al.*, 1992; Shirai *et al.*, 1999; Yazawa *et al.*, 1991). They grew the first InAs nanowires as small as 20nm in diameter on GaAs substrate (Yazawa *et al.*, 1991), despite the large lattice mismatch. These authors observed growth of wurtzite InAs with In as possible catalyst metal, which is in essence the self-catalyzed growth, as is called today.

The resurgence of nanowire research occurred about 10 years ago as indicated by a ''threshold'' in the plot of numbers of papers on nanowires as a function of time (Yang *et al.*, 2010). Since then, nanowire growth has been demonstrated in almost all kinds of semiconductors, from elemental, compound, to various alloys, from III–V, II–VI, to IV–VI, and from nitrides to all types of metal oxides, using almost any known crystal growth method, from chemical vapor deposition (CVD), physical vapor deposition, metalorganic CVD (MOCVD), and molecular beam epitaxy (MBE). This chapter will not focus on the growth, as many excellent

review papers on various growth approaches and mechanisms exist already (Duan and Lieber, 2000; Fan *et al*., 2006; Gao *et al*., 2011; Hu *et al*., 1999; Joyce *et al*., 2011; Lauhon *et al*., 2004; Moore and Wang, 2006; Pan *et al*., 2011; Pauzauskie and Yang, 2006; Samuelson, 2003; Sirbuly *et al*., 2005a; Thelander *et al*., 2006; Tomioka *et al*., 2011; Wang, 2009; Yang *et al*., 2002), including many other excellent papers in the recent special issue mentioned above (Jagadish *et al*., 2011).

Several advantages of nanowires in connection with their growth and material quality are worth mentioning here. One of the advantages of nanowires seems to be the insensitivity of material quality to the growth equipment used. Even though expensive equipment such as commercial grade MBE or MOCVD has better controls and is generally preferred, evidence suggests that there is almost no difference of material quality between nanowires grown by commercial grade MBE or MOCVD and those by simple, inexpensive tube reactors.

Surface states are very often mentioned as one of the most severe issues for nanowires due to the large surface to volume ratio. But it is interesting to point out that the issue can turn out to be a better attribute for nanowires. Due to the small cross-section, defects (such as impurities, vacancies) or any other inhomogeneities are more likely to form only near or on surfaces, leaving the large interior of the wire body largely defect-free. Such near-surface states are more easily removed from nanowires than from bulk materials using surface treatment or annealing in certain environments. Once treated, the entire wire (including interior and surfaces) is high-quality optical material. This is especially important for materials that are more prone to defect (such as vacancies) formation when grown into bulk or thin-film form. The more or less uniform distribution of defects and impurities in the interior of bulk materials makes them very difficult to remove. This is why high-quality nanowire materials with very minimum midgap emission have been demonstrated for ZnCdSSe material system when growth condition is optimized. This also explains why material quality of nanowires is largely insensitive to the growth equipment as we mentioned earlier.

Nanowires can be grown either epitaxially from a single crystal substrate or they can be grown with complete random orientation without any directional relationship with the substrate. In the former case, the lattice mismatch between the wire materials and substrates can be significantly larger than the planar epitaxial technologies, due to the small contact area between wires and the substrate. In the latter case, substrates simply serve as a mechanical support and thus there is no requirement of lattice matching. As a result, substrate choice is no longer as critical an issue as in the case of planar epitaxial growth. Such advantage has huge implications for optoelectronic applications, since we have a much wider array of material choices that are not available for planar epitaxial growth.

In principle, any compounds or alloys can be grown on any substrate as long as they are possible in terms of material chemistry. In terms of lasers and light-emission devices, this means an unprecedented availability of wavelengths.

Most of the wires discussed so far are made using bottom-up approaches based on the VLS growth mechanism. While bottom-up approaches have achieved great success over the past 10 years, there are still issues and challenges related to the wafer-scale manufacturability and yield, especially in the intermediate steps between growth and device fabrication. With the constant progress made in the top-down nanofabrication processes, it has become also possible to etch similar nanostructures from fabricated wafers using the top-down approach. It was recently demonstrated that very complicated structures can be produced in vertical arrays of wires with sizes in the range of 20–40 nm (Wang *et al.*, 2011). The advantage of such an approach is that it can benefit greatly from the more mature planar epitaxial growth technology that can produce highly controlled multilayer structures with well-controlled doping profiles on a wafer scale. There are several advantages in the specific top-down approach demonstrated by Wang *et al.* (2011): The self-masking effect leads to mask-free fabrication process – and could significantly simplify the fabrication – and leads to high yield with low cost in the long run. Second, the posttreatment after the etching was extremely effective in removing the surface damages and in recovering the intrinsic quality of photoluminescence (PL). As a result, high-quality vertical wire arrays were produced with high density, with the sophisticated longitudinal structures along the wires built in during the epitaxial wafer growth process. Such structures can be then further processed into array of devices following processing steps similar to those used by Hill *et al.* (2007, 2009).

3. LASING OF NITRIDE NANOWIRES

Nitrides are among the first and most often studied nanowires for lasing applications. Johnson *et al.* (2002) demonstrated the first lasing of individual GaN NWs using a combination of near-field and far-field optical microscopy to characterize the waveguide mode structure and spectral properties of emission at room temperature. Optical microscope images revealed mode patterns associated with axial Fabry–Perot modes of the cylindrical cavity geometry of the monocrystalline nanowires, with Q-factor as high as 1000. The sizes of NWs are in the range of 150–300 nm in diameter and 30–40 μm in length. This study contributed significantly toward the establishment of modal relationship between mode pattern and spectral contents with the mode structures of a cylindrical dielectric

waveguide and represented a considerable initial advance toward the understanding of nanowire-based lasers.

Lasing in more sophisticated GaN/InGaN multiple quantum well structures of a triangle cross-section was demonstrated by Qian *et al.* (2008) under optical pumping. By changing the In-composition of quantum wells of different structures, several lasing wavelengths in the range of ~400–500nm were achieved from individual core–multishell structures. Over 20 quantum wells were realized in the radial direction, representing state of the art of the fabrication capability with great control. Even though only optical pumping was demonstrated, it would be interesting to see if electrical injection lasing can be achieved using these structures.

In a very interesting recent study (Das *et al.*, 2011), a single GaN nanowire, 60nm in diameter and 750nm in length, was embedded in a SiO/TiO distributed Brag reflector cavity. Under increasing optical pumping, the authors observed two thresholds at room temperature: one at 92.5 nJ/cm^2 and another at 250 $\mu J/cm^2$. Associated with each of the thresholds, there is a superlinear increase of integrated intensity and a dramatic decrease of linewidth down to 1.1 and 2.5meV, respectively. The dramatic decrease of emission linewidth from ~10meV of A-exciton below threshold to ~1meV represented a dramatic photon condensation to the cavity mode, even though the linewidth of the cold cavity was not given. The first threshold was interpreted as corresponding to the polariton lasing, while the second one to the regular photon lasing of electron-hole plasma. The overall linewidth showed a double-dip behavior as a function of pumping power. The second threshold is accompanied by a decrease and then saturation of linewidth at low level, a typical behavior seen in regular laser threshold. The linewidth only shows a sharp dip near first threshold without apparent stabilization at the small value. It would be interesting to compare the minimum linewidth near the first threshold with that of the cold cavity. In addition, the angle-resolved PL seems to agree with the theoretical dispersion curves expected from the polariton mode.

In another related work, Heo *et al.* (2011) studied lasing from a single GaN NW with size of 20–50nm in diameter and 600nm in length. The NW stands inside a defect of a photonic crystal structure that was fabricated around the NW. The GaN nanowires were first grown on Si substrate with Ga seed particles sparsely distributed on the substrate. The vertical NWs on Si substrate were then coated with spin-on glass of 380nm thickness to act as an isolating layer so that light is not too strongly coupled to the Si substrate. A layer of 120-nm-thick TiO_2 was then deposited by electron beam evaporation. Finally, photonic crystal structure was fabricated using electron beam lithography into TiO_2 layer. The authors estimated a cavity Q of 570 and required a threshold material gain of 13,000 cm^{-1}. Lasing was demonstrated under optical pumping with a

threshold around 140 kW/cm^2 and a linewidth of 0.55 nm. This linewidth at a central wavelength of 371 nm corresponds to a lasing Q-factor of 670, which is only slightly larger than the Q of 570 for the cold cavity. One additional interesting aspect of this work is that the NWs are grown on Si substrate.

Nitride nanowire lasing was also the subject of comprehensive theoretical and simulation study by Maslov and Ning (2007c), where many of the discussions and results are applicable to nanowire lasers in general. Even though major results had been published elsewhere (Maslov and Ning 2003, 2004a,b,c, 2006, 2007c), the book chapter of Maslov and Ning (2007c) provides more extensive and complete discussions of many topics related to GaN NW lasers.

4. LASING IN GROUP II–VI COMPOUND AND ALLOY NANOWIRES

Various compounds and alloys of groups II and VI elements have been studied quite extensively for optoelectronic and lasing purposes. Other aspects of lasing using these materials will also be discussed in connection with widely tunable lasing (Section 5) and lasing in coupled nanowires (Section 8).

4.1. Lasing study in ZnS nanowires and nanobelts

ZnS is among the most often studied II–VI compounds; for a review see Moore and Wang (2006). Ding *et al*. (2004) demonstrated PL in ZnS array nanowires grown in an anodic aluminum oxide (AAO) template. They observed a linewidth of 2.2 nm with a central wavelength around 338 nm. Even though the overall linewidth seems to be broad, sub-nanometer features were observed on top of the broad peak. Since the individual wires are very small (~25 nm in diameter), the modes are likely resulted from coupling of some sort, or collective behavior of many wires. At almost the same time, the same group (Zapien *et al*., 2004) studied in detail and presented interesting results about the lasing properties of individual wurtzite ZnS nanobelts with dimensions of several tens of microns in length, several microns in width, and 100 nm in thickness. They used a fiber of 1.2 mm in diameter to measure the PL of a nanoribbon by placing it at different distances: 2 and 40 mm. The angle of the collection cone (ACC) was estimated to be around 30° and 2°, respectively. They obtained very broadband emission even at high pumping and the linewidth was 2 nm for the large ACC. Such a linewidth is much broader than what one expects from a laser of this wavelength, since this means a Q-factor of 169 of the lasing line. But the integrated PL versus pumping

showed a clear threshold. Interestingly, features of sharp peaks were observed without spontaneous emission background for small ACC with a linewidth as narrow as 0.1nm, which corresponds to a Q-factor of 3380. The measurement results presented in this chapter demonstrate the important roles of the details of collection arrangement in a nanolaser. The strong presence of the spontaneous emission in the signal collected with a large ACC could mask the real lasing features. This is likely one of the reasons that many lasing spectra of nanolasers show broader peak than expected. Similarly, narrow peak *per se* is not enough evidence for lasing either, since a high Q resonator can show a spectral line as a passive filter. Other corroborating evidence is needed, such as integrated intensity with pumping power. In addition, significant linewidth narrowing is necessary with increasing level of pumping. There is one additional reason why size of collection cone is important. As was shown theoretically by Maslov and Ning (2004b), different modes could have very different far-field propagation directions. A small ACC will miss certain modes. This is due to the very small size and strong confinement of modes.

4.2. ZnCdS nanoribbons

ZnCdS nanoribbons of wurtzite structure were synthesized (Liu *et al.*, 2005) using laser ablation CVD with thickness around 50–80nm, width 0.5–5μm, and length on the orders of hundreds of microns. Alloy composition changes with substrate temperature allowed 25% variation of ZnCdS from the CdS end and similar ∼25% from the ZnS end, resulting light emission in the 485–515 and 340–390nm bands, respectively. Narrow spectral lines were observed and interpreted as corresponding to the modes of nanoribbon cavities after the subtraction of a broad Gaussian background from the overall PL spectrum. For lasing demonstration, it is often important to show such narrow peaks of one or few modes at high enough pumping as a result of mode competition without subtracting the broad background.

4.3. CdS and CdSSe nanowires and nanoribbons

Agarwal *et al*. (2005) demonstrated single NW lasing using CdS with exciton–exciton scatterings identified as a lasing mechanism for temperature range up to 75K. The NWs sizes are in the range of 80–150nm in diameter and 30–50μm in length. Lasing wavelength changes from 490nm at 4K to ∼500nm at 200K.

In addition to binary compounds, lasing in ternary alloy nanowires was the topic of extensive study. The first experimental demonstration of PL emission in the complete bandgap range of alloy CdSSe was reported

by Pan *et al*. (2005) between 510nm (CdS) and 710nm (CdSe). Similar to Liu *et al*. (2005), these authors utilized the temperature gradient inside a tube reactor and placed several Si substrates in different temperature zones to collect nanobelt samples of different alloy compositions. High-quality PL with uniform features was collected from all regions, with somewhat broader and weaker PL from the samples near the CdSe end of the alloys. Temperatures increasing from 650 to 800°C were recorded for furnace positions of pure CdS to pure CdSe with increasing Se composition. In follow-up research, these authors (Pan *et al*., 2006) demonstrated the growth of large whiskers of 600 by 5000nm in cross-section and 100s of microns in length. Such large whiskers are obviously very good optical cavities and thus were able to lase at high-optical pumping. This was the first demonstration of alloy CdSSe lasing in the complete composition range between CdS and CdSe, even though the sizes of whiskers were quite large. The cross-section of the whiskers is 5–12 times as large as the wavelengths squared. In addition, the samples were collected from several substrates placed at different locations.

Single crystal wurtzite nanoribbons of CdSSe alloy were fabricated (Liu *et al*., 2007) through a combination of laser ablation and thermal evaporation. Several substrates were placed between two temperature zones at different locations with different temperatures in the range between 450 and 600°C. Different substrate temperatures allowed the growth of alloys of different compositions in the full composition range between CdSe and CdS. The dimensions of nanoribbons are 0.4–10μm in width, 65–80nm in thickness, and several hundreds of microns in length. Samples collected from these substrates were analyzed using various means including optical studies. Light emission was observed from 510 to 710nm. At higher level of pumping, many of the PL spectra become lasing with much sharper spectral peaks. Even though some PL spectra showed broader linewidth, the authors demonstrated that sharp lines with full width at half maximum (FWHM) around ∼0.6nm appeared after the removal of a broad background of a Gaussian shape. Since the Gaussian background represents obviously spontaneous emission, an interesting question is if such narrow lines represent cold-cavity modes or lasing lines. Quantitatively, 0.6nm would represent a Q of ∼1000 for wavelength around 600nm. Due to the large size of nanoribbons, such a cavity Q-factor is possible. A very important piece of information would be the pump dependence of linewidth, as mentioned earlier. Significant linewidth decrease by a factor of 10 is typically expected from the cold-cavity value near the laser threshold. Another interesting and intriguing aspect to note is that the thickness of the nanobelts is in the range of 65–80nm. Assuming the refractive index of ∼2.5, the optical thickness of such nanobelts is only 160–200nm, less than half of the shortest wavelength involved. Details of the measurement substrates and other environmental

aspects need to be known to understand the wave-guiding mechanism and the results of optical measurements. Another interesting observation is the ability of fine-tuning of the alloy composition and the associated PL peak position on the order of a few nanometers. In a more recent study, Li *et al.* (2009) demonstrated a novel method of producing CdSSe alloy nanoribbons by a two-step process of first growing CdSe nanoribbons and the subsequent sulfurization. The authors demonstrated that controllable alloy composition can be achieved through annealing time and temperature. Tunable PL was observed with linewidth on the order of a few nanometers with the accompanying cavity modes.

It was pointed out by Zapien *et al.* (2007) that the two alloy samples of CdSSe and ZnCdS each can continuously lase in the wavelength ranges of 340–510 and 510–710nm, respectively. Therefore, the two material systems, if combined together, could provide lasing in an extremely broad wavelength range between 340 and 710nm. As an example, they presented lasing at 340, 393, and 495nm from a ZnCdS sample and 575, 634, and 710nm from a separate CdSSe sample. It would be more interesting if such a broadly tunable lasing could be achieved on a single substrate in a single run of growth in the entire range of 340–710nm. Only more recently has such broadly tunable light emission (not lasing) been achieved in the entire wavelength range between 340 and 710nm using quaternary alloy nanowires grown by the dual gradient method (Pan *et al.*, 2009b, 2010).

5. WIDELY TUNABLE NANOWIRE LASING AND EMISSION FROM A SINGLE SUBSTRATE

5.1. Lasing in ternary alloys grown using temperature gradient

The early investigations clearly showed that substrate temperature is one of the most important growth parameters to control the alloy compositions in the growth of ternary alloy nanowires, nanobelts, and microwhiskers, and the demonstration of light emission or lasing in a wide range of wavelengths (Liu *et al.*, 2005, 2007; Pan *et al.*, 2005, 2006; Zapien *et al.*, 2007). Even though it was known that different alloy compositions require different optimum substrate temperatures, it was important to show that the required temperatures to grow the complete alloy composition range between CdS and CdSe could be all realized in a single CVD setup (Liu *et al.*, 2005, 2007; Pan *et al.*, 2005, 2006). From device application point of view, a *tunable* light source very often means a single device that can be produced in a monolithic way on single substrate and the *tunability* is realized by a simple change of a parameter. But in these early studies, several substrates were used with unspecified spatial arrangements (Pan

et al., 2005, 2006), or samples from different growth experiments were measured (Zapien *et al.*, 2007). Sometimes samples were removed from the original growth substrates for various measurements so that the spatial information was lost or not provided. In addition, a systematic attempt was needed to relate spatial temperature distribution to local alloy composition, bandgaps of alloys, and the eventual wavelengths.

To explore, in a systematical fashion, the possibility of growing the entire alloy composition range from CdS to CdSe on a single substrate, a custom-designed single-zone CVD setup with an intentionally large temperature gradient was used (Pan *et al.*, 2009a) such that temperature can vary between 580 and 690°C over a length of 1.2cm. There was a careful optimization involved such that high- and low-temperature ends of the substrate were appropriate for the nanowire growth of the binary ends, CdSe and CdS, while all the intermediate temperature zones are suited for the growth of ternary CdS_xSe_{1-x} with x increasing from 0 to 1 from high to low temperatures. Spatial-resolved temperature measurements were then correlated with the micro-XRD (X-ray diffraction), SEM–EDX, and micro-PL. Molar fraction extracted from the SEM–EDX measurement provides a spatially resolved alloy composition map along the length of the original substrate. Using the well-known Vegard's law, bandgaps of various alloy compositions at various spatial locations can be constructed. Such bandgap spatial map can then be compared with micro-PL peaks. Excellent agreement was obtained between the extracted bandgap and PL peaks, indicating the PL peak tuning is a result of alloy composition grading. Such spatial-resolved structural, compositional, and optical measurements are important in establishing the relationship between the temperature gradient and spatial grading of alloy composition, and for purposeful production of alloys of given composition in the future. Under stronger optical excitation, we were able to demonstrate (Pan *et al.*, 2009a) spatially tunable lasing from the as-grown samples on the original substrate. We emphasize the importance of the optical measurements without transferring samples to other substrates or taking samples from several different substrates, since, for many practical applications, it is much more preferred to have a single tunable device with a wide range of wavelength tunability than from several separate substrates or devices. CdSSe alloy nanowires on a single substrate was the widest wavelength-tunable lasing of any semiconductor laser ever realized on a single substrate with a relative tunability of $\Delta\lambda/\lambda = 200/600 = 1/3$. With such materials capability, it can be imagined that the entire substrate can be subdivided along the length into N cells with each cell having a specific wavelength range and with separate pair of electrical contacts. By sequentially turning each cell on and off, wavelength can be tuned in the entire wavelength range of 200nm by pure electrical means. Within each cell, wavelength can be further fine-tuned through thermal or electrical

means, as is usually done in a semiconductor laser. Such a truly widely tunable laser would be extremely useful for multiagent detection system, or for on-chip electrical-to-optical, or optical-to-optical multiplexing applications in a communication system.

5.2. Quaternary alloy nanowires with tunable emission over the entire visible spectrum

As pointed out by Zapien *et al*. (2007), combining ternary alloys of ZnCdS with CdSSe could provide light emission or lasing in the entire visible spectrum. But it is a nontrivial matter to actually grow such a single sample (not several individual samples) with the wide range of alloy compositions to bridge ZnCdS and CdSSe. Actually it turned out that there was no need to combine the two ternaries. A complete composition range from alloying the binaries ZnS and CdSe would provide exactly the needed bandgap range. A generic alloy of ZnS and CdSe in its most general form would lead to quaternary alloys of ZnCdSSe type. It is interesting to note that, as it turned out, while quaternary alloys of various sorts have been realized in thin-film form or quantum wells, quaternary alloys in any nano-form (nanowires or quantum dots) had not been reported until 2009 when our group first grew ZnCdSSe nanowires and nanobelts (Pan *et al*., 2009b). By controlling relative molar fractions between ZnS and CdSe in the source material, we were able to grow various compositions of ZnCdSSe alloy such that wavelengths of the light emission can change between 350 and 710nm (Pan *et al*., 2010), or between the bandgap emission wavelengths of ZnS and that of CdSe. While such a result is an exciting first step, this is not yet wavelength-tunable emission in the sense that different compositions had to be realized in different samples separately.

While temperature gradient method (TGM) was very successful in growing the CdSSe alloy, it turned out that TGM alone was not sufficient for growing entire composition range from CdSe to ZnS on a single substrate, as our repeated experiments using TGM alone achieved only certain ternaries. In the meantime, InGaN alloy was grown for the first time (Kuykendall *et al*., 2007) in the entire composition range using a modified CVD setup where multiple minitubes inside a large horizontal tube reactor were used to transport separate source elements. A growth substrate was placed vertically in the low-temperature zone down the stream of vapor transport. Since temperature inhomogeneity inside a horizontal reactor is mostly horizontal, the vertically oriented substrate had nominally the uniform temperature across its length. In that specific setup, chlorides of indium and gallium were placed inside separate minitubes and transported down to the substrate side in mutual isolation until they reach the ends of respective tubes.

A common ammonia source was shared in a third tube. Through the adjustment of the separation of the two chloride minitubes, profiles of In and Ga elements onto the substrate can be adjusted. It is generally expected that one end of the substrate would receive mostly Ga and N, the opposing end mostly In and N. In the intermediate range, different mixed ratios of Ga and In would result in different alloy composition upon growth. The essence of this method is to create a gradient of elemental compositions on the growth substrate from top to bottom. Thus we call this the elemental composition gradient (ECG) method, in contrast to TGM. Various attempts of using such an ECG alone was not successful in growing ZnCdSSe alloy in the complete composition range either.

It is then natural to combine TGM with ECG. Such a dual gradient method (DGM) is illustrated in Fig. 12.1, where separate minitubes are used to transport ZnS and CdSe as was done by Kuykendall *et al*. (2007) for Ga and In. But unlike Kuykendal *et al.* where substrate was vertical, the substrate is no longer perpendicular to the axis of the reactor, such that a temperature gradient of a significant value is purposely introduced and optimized. The DGM turned out to be an extremely powerful approach that allows more freedom for the growth optimization, and

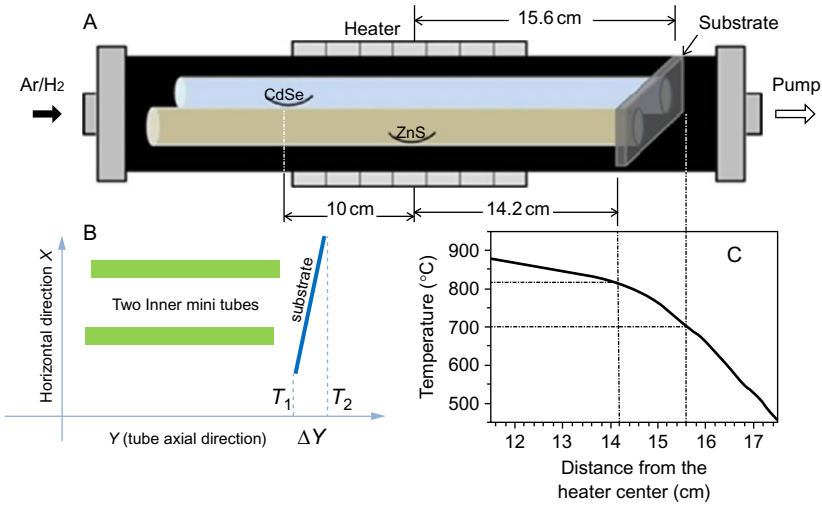

FIGURE 12.1 Schematic CVD setup using the dual gradient method (A), a top view (B) showing the relative orientations of the two minitubes and the tilted substrate with both ends having different temperatures, and actual temperature distribution in a small segment near the tube exit showing the temperature gradient across the length of the substrate (C).

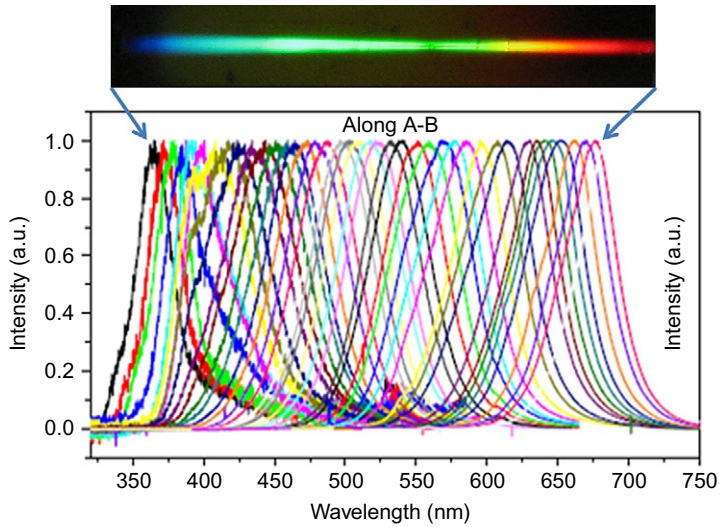

FIGURE 12.2 Real-color photograph of the composition-graded nanowire sample under a UV light illumination (top) and 40 spectra of micro-photoluminescence measured at 40 locations along the length of the substrate (bottom).

eventual realization of composition-graded alloy nanowires in the entire range from ZnS to CdSe. An example of nanowire samples is shown in Fig. 12.2, where real-colored PL image from the as-grown sample is shown. The detailed micro-PL measurements along the substrate shown in the same figure confirm that the color change is from the bandgap change across the substrate. Detailed characterization of the materials compositions through micro-XRD, high-resolution transmission electron microscopy (TEM), and TEM energy dispersive X-ray scattering (TEM–EDX) all agree with the PL measurements being from the band-edge emission of the corresponding quaternary alloys. Another interesting feature of the PL result is the relative weak emission originated from the below-bandgap states that are very typical of wide gap materials. We believe that the optimization of local temperature is largely responsible for the high quality of the materials and good uniformity of morphology. In addition, the DGM also allows the grading of alloy composition along both directions on a substrate, achieving two-dimensional compositional control. Such two-dimensional DGM samples also provide a library of quaternary alloys for studying various material properties of the alloys. The DGM is a powerful approach that can be used to further optimize the size and quality of nanowires or nanobelts. More systematic research is needed to eventually demonstrate widely tunable lasing from $\sim$350 to $\sim$710nm on a single substrate.

6. LASING OF ZnO NANOWIRES AND NANOBELTS

ZnO nanostructures such as nanowires and nanobelts have been of great interest from a variety of perspectives. A comprehensive recent review was presented by Wang (2009) on almost every aspect of ZnO nanostructures from growth of various morphologies to a wide range of applications. A review dedicated solely to ZnO nanowire lasers also became available recently (Vanmaekelbergh and van Vugt, 2011).

6.1. Lasing in nanowire arrays

The first demonstration of lasing by NWs was made using ZnO NWs by Huang *et al*. (2001), where it was argued for the first time that semiconductor NWs can form natural laser cavities, thus opening the new era of nanowire lasers. The diameters of wires varied from 20 to 150 nm, while lengths were up to 10 μm. Under optical excitation at room temperature, lasing action was observed at 385 nm, with an emission linewidth less than 0.3 nm. This research represents an interesting development in the history of lasers in several senses: First, the cross-section of nanowires was orders of magnitude smaller than the microlasers that were the frontier of laser research at the time. Second, this was a radically different type of laser cavity with a quasi-one-dimensional structure where small wire ends play the role of reflectors, but with a size much smaller than the wavelengths involved. Even though the detailed quantitative understanding turned out to be somewhat different (Maslov and Ning 2003), the revelation that such small facets can be good enough reflectors was very important. Third, this demonstration started the whole new field of nanowire lasers, which has since attracted more and more attention from various communities. The demonstration of lasing in a two-dimensional array was quickly followed by one-dimensional dendritic array of ZnO nanowires by the same group (Yan *et al*., 2003a). Unlike the two-dimensional array, such dendritic structure was a nanolaser array with regular spacing in the range of 0.1–2 μm and diameter in the range of 10–300 nm. Array mode spectral narrowing was observed together with spatial-resolved imaging of individual wires.

6.2. Lasing of individual ZnO NWs or nanoribbons

While lasing from ZnO nanowire arrays initiated the new field of nanowire lasers, there were certain open questions such as the role of individual nanowires, the exact mechanisms of lasing, and if any collective effects were responsible for lasing. Many of these questions were answered by Johnson *et al*. (2001) which demonstrated lasing in single

ZnO nanowires of 40–150nm in diameter and 4–10μm in lengths. The linewidth of lasing modes is between 1 and 3nm for central mode wavelength around 380nm.

A very detailed measurement of integrated light intensity from a ZnO nanowire as function of pumping power was carried out more recently by Zimmler *et al*. (2008), where the entire ''S'' curve from below to well above the threshold was characterized. In particular, the transition from superlinear regime (threshold region) to linear region (above threshold) was observed. This feature is important in demonstrating the full transition from below to above threshold and was not always presented in earlier work. A threshold value of 270kW/cm^2 was estimated for a nanowire of 12.2μm in length and 250nm in diameter. The linewidth is around 0.4nm in the threshold region, even though no linewidth information was presented well above threshold or as a function of pumping. The authors also measured various wires of a range of sizes and found that the wire diameter smaller than 150nm could not lase. Another interesting attempt was made by partially suspending one portion of the wire in air so that direct measurement along the wire axis direction could be taken. Total output power can be then measured in absolute unit. More detailed and systematic study by the same group was later reported in a review article (Zimmler *et al*., 2010), where more detailed analysis of modes and reflectivities of wire facets were made, including the effects of wire-on-substrate geometry. One of the important theoretical results was the threshold gain as function of the NW diameter for various wire lengths. For all the wire lengths, the threshold material gain increases dramatically for diameter smaller than 100nm for the HE_{11} mode, the lowest order mode for the cylindrical geometry. The threshold approaches or exceeds 10,000cm^{-1}, a value that becomes prohibitive for most gain materials to reach. Near the cutoff diameter of the TE_{01} mode, the HE_{11} mode has smaller threshold gain, but above the cutoff diameter, the TE_{01} mode threshold gain drops quickly to below that of HE_{11} mode; this is why TE_{01} mode becomes very often the lasing mode. This verified the prediction made earlier (Maslov and Ning, 2004b,c, 2007c). The threshold gain for TE_{01} mode is generally below 1000cm^{-1} above cutoff size, achievable for ZnO and many other materials. The head-on geometry also allowed the first measurement of the far-field properties of individual nanowire lasers, with measurement results largely in agreement with those predicted earlier (Maslov and Ning 2004a). The maximum emission angles of far fields of TE_{01} and TM_{01} appear off the wire axis at angles between 30° and 50°. In addition, this chapter also contains detailed study of temperature dependence and the gain mechanism in ZnO in general, as this is a rich field of study and a quite complex subject for ZnO.

While most of the studies for the individual nanowire lasers were carried out by transferring nanowires to a different substrate where

wires are lying horizontally (Yan *et al*., 2003b; Zimmler *et al*., 2008), there are a few issues associated with this configuration. First the contact of the side walls of nanowires with substrate very often change the cavity structure completely and therefore the mode structures. The usage of high refractive index substrates often reduced the index contrast between the wires and substrate significantly, leading to large loss through the substrate. In addition, the measurement of the far-field pattern becomes complicated. To improve the situation, Gargas *et al*. (2009) recently intentionally grew ZnO nanowires with controlled small density such that each nanowire could be individually probed while vertically standing on the original substrate. In addition, the usage of UV-laser scanning confocal microscope allowed three-dimensional imaging of laser field along the nanowires. Such sectioning could provide important information about the true three-dimensional mode structures.

7. INFRARED AND LONG-WAVELENGTH LASING

Vast majority of the nanowire lasers demonstrated so far are in the UV or visible wavelength ranges. Nanolasers in the infrared wavelengths are expected to be important due to many potential applications in the future chip-scale optical interconnects and integrated nanophotonic systems for detection, sensing, and information technology. There are some differences between visible and infrared wavelengths and associated obstacles for infrared lasing. Due to the increased wavelengths, infrared optical applications require relatively large size of nanowires for decent waveguiding, as can be seen from a normalized modal dispersion relationship (Maslov and Ning, 2003). Second, nonradiative recombinations such as Auger processes become more severe in the infrared due to reduced bandgaps. Third, infrared detection is more complicated, less widely available, and less sensitive, especially for mid-infrared wavelength ranges and longer.

The first infrared lasing was demonstrated (Chin *et al*., 2006) using GaSb wires with diameters in the range of 700–1500 nm and lengths of 10–70 μm dispersed on a sapphire substrate. GaSb is an interesting material, since its bandgap emission falls within the communication wavelength bands around λ=1550 nm at low temperature. With a large refractive index of n=3.8, the wavelength in GaSb, λ/n, is around 410 nm so that any wires with diameter larger than 400 nm would be a good waveguide in air. Details of wire growth and related study are reported in (Vaddiraju *et al*., 2007). Briefly, the wires were grown using a self-catalyzed method with Gallium drop on quartz substrate as both the Gallium source and catalyst. Antimony was provided from a solid antimony source or from antimony chloride. The dissolution of antimony into gallium and

subsequent supersaturation leads to the nucleation of GaSb. As a result, the wires are very often grown out of large pieces of gallium. The wires are removed from the quartz substrate after the growth and dispersed onto sapphire substrate for optical characterization. Under strong optical pumping, lasing was observed in various wires of different sizes up to ∼30K. For most of lasing demonstration, the central wavelength is around 1550nm, with linewidth as narrow as ∼2nm.

Lasing in single GaAs/GaAsP core–shell nanowire structures was recently demonstrated around wavelength of 815nm at low temperature (Hua *et al.*, 2009). The structures were grown using selective area epitaxy in an MOCVD system on GaAs (111) substrate, with diameters of 200–500nm and lengths of 2–6μm. The lasing linewidth was in the range of 0.8–1.5nm at 4.2K. Although spectra were shown up to 125K, the spectra were significantly wider above 50K. The high threshold is probably due to the relatively small size of the structures for this wavelength.

Another infrared lasing was demonstrated more recently on Si substrate. Even though nanowires and nanopillars of III–V materials such as InP and GaAs had been grown on Si substrate before, direct lasing from the as-grown nanopillars on the original silicon substrate represented an important development (Chen *et al.*, 2011). These authors grew InGaAs nanopillars with GaAs shells on Si (111) substrate. They demonstrated lasing around ∼900nm central wavelength variable within 50nm by using slightly different In-compositions in the core. The nanopillars have diameters 550–700nm and length of 3–5μm. Due to the leakage into the high-index Si substrate, lower-order modes which experience large loss did not lase. Higher-order whispering gallery modes can, however, lase, since they experience less leakage loss due to larger incidence angles onto the Si-interface. As a result, such modes can lase up to room temperature with relatively small cavity Q around 200. Such III–V nanopillars directly grown on Si could potentially be interesting since it overcomes several obstacles of the traditional III–V-Si integration: large lattice mismatch and difference in processing temperatures. The small footprint of nanopillars would also allow more adaptive changes under changing thermal conditions and make the difference in thermal properties of III–V and Si less serious an issue.

For longer wavelength lasing in nanowires in mid-infrared, the traditional lead salt materials provide interesting candidates. Lead sulfide (PbS) has a bandgap around 0.42eV at room temperature. Quasi-one-dimensional wire structures have been grown by a few groups (Bierman *et al.*, 2007; Nichols *et al.*, 2011) using VLS approach in a CVD system. Relatively large wires are typically grown with diameters from hundreds of nanometers to a few microns with length on the order of tens of microns. PbS is an interesting semiconductor gain material in the mid-infrared, because of several reasons: First, Auger processes are typically the most important nonradiative recombination processes in narrow gap semiconductors to compete with light-emission processes. The almost-same effective masses of

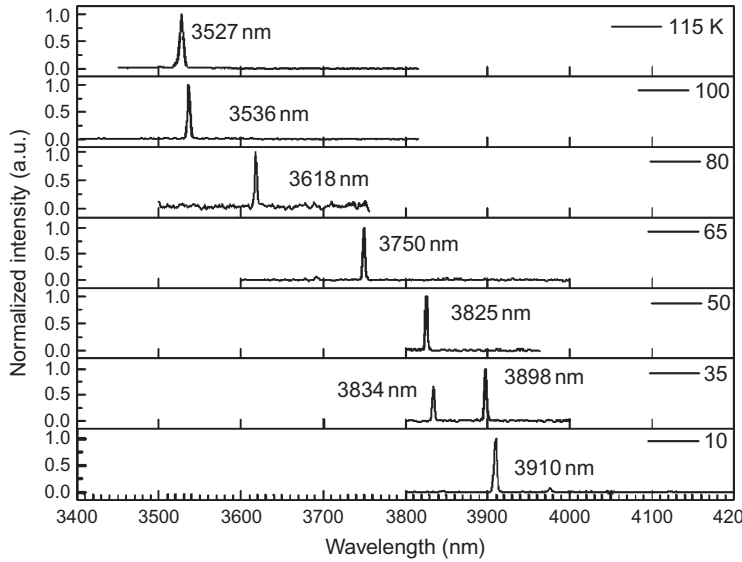

FIGURE 12.3 Lasing spectrum of a single PbS wire under pumping by a Ti:sapphire laser at various temperatures, demonstrating the first lasing of single PbS wires, with blue shifting of lasing modes with temperature due to the expected increase of bandgap (from Sun *et al.*, 2011).

conduction and valence bands of PbS mean that the Auger processes are much weaker than in materials of similar bandgaps with significantly asymmetric masses such as InAs. Second, the large dielectric constant of PbS (around 18 vs. 12 for InAs) means stronger screening of Coulomb interaction or weaker processes that depends on Coulomb potential, such as Auger processes, which are proportional to the second order in Coulomb potential. As a result, PbS wires show stronger light emission than InAs. Shown in Fig. 12.3 are emission spectra of a single PbS wire under pumping by a 790-nm Ti:Sapphire mode-locked femtosecond laser at different temperatures from 10 to 115K (Sun *et al.*, 2011). As temperature rises, we see a clear emission wavelength shifting to shorter wavelengths from 3910 to 3527 nm, due to the known bandgap increase with temperature. This is contrary to the typical III–V or II–VI semiconductors where bandgap shrinks with increasing temperature. The linewidth is typically around 3–4nm.

8. LASING FROM COUPLED NANOWIRES

Coupling of nanowires through evanescent field have been explored for various applications including lasing and LED demonstrations with some interesting phenomena observed. These include both coupling of

different parts of a single nanowire (self-coupling) and coupling of different nanowires (mutual coupling).

One early demonstration of coupled nanowires involved organizing nanowires into coupled crossbar networks. InP nanowires (Duan *et al.*, 2001) of n- and p-types were assembled to cross each other, such that a p–n junction is formed at the intersection points. As a result, PL and electroluminescence were observed at the cross-point, demonstrating basic LED operation. In a slightly different approach, solution-based synthesis was used to produce nanowires of various materials (such as GaN, CdS, and CdSe) with different bandgaps by Huang *et al.* (2005). Such n-type doped NWs are then organized into crossbar configuration with p-doped Si NWs. In this way, two-dimensional array of LEDs were demonstrated with various colors.

Huang *et al.* (2007) studied theoretically the coupling of two parallel nanowires and analyzed coupling efficiency. Due to high refractive index of nanowires and the tighter field confinement, coupling of nanowires requires smaller distance and very often shows strong coupling at small distance. Xiao *et al.* (2011a) demonstrated single-mode lasing using two CdS nanowires of 420 nm in diameter arranged in *x*-form with a linewidth ~0.1 nm. While the single straight nanowire without forming such structure would show multimode lasing, the mode selection is realized through the coupling of the cavities.

In terms of self-coupling, the simplest form is to reconnect both ends of nanowires with a certain length overlapping. Individual nanowire ring lasers were demonstrated by looping long GaN NWs and reconnecting the two ends with overlapping segments (Pauzauskie *et al.*, 2006). The authors systematically compared PL and lasing between straight wires and looped rings made of wires of the same lengths. Several interesting features were observed: (1) PL peak positions shift consistently to the red in the looped wires, (2) more pronounced mode structures are observed in looped ring structures than in straight wires, and (3) larger *Q*-factor is observed for rings than for straight wires. All these were explained by the additional feedback through the looped coupling, as compared to the straight wires. The redshift of the PL peaks turned out to be a result of quite subtle effects of evanescent coupling which favors longer wavelength due to the existence of gaps in the overlapping segments. Beside many intrinsic features observed in this work, the idea of looping nanowires to form better cavities using the same wires with the same volume of gain materials may serve as a general strategy for making smaller lasers or making nanowire lasers with shorter wires. This idea is further explored in follow-up work recently by Xiao *et al.* (2011b). These authors compared systematically three different cases: (1) a nanowire with both ends open, (2) a nanowire with one end looped, and (3) nanowire with both ends looped. The CdSe nanowires studied have dimensions of

200 nm in diameter and 50 μm in length. Several findings are indeed very interesting. First these authors observed the selection of a single mode when one or both ends of nanowires are looped and the side-mode suppression becomes stronger when both ends are looped. Second, the lasing threshold decreases by almost half when one of the ends is looped compared to the case when both ends are open. The threshold decreases to about one-third when both ends are looped. Obviously, the reflectivity is dramatically increased by simply looping one or both ends of a wire back to itself. The reflectivity changes from the standard lower value of 30–40% (Maslov and Ning 2003) to almost 100% in an ideal looped case. Evidently the looping itself will introduce some bending loss and scattering loss at the reconnection section. Both the side-mode suppression and threshold reduction enabled by the looping are very important for applications of nanowire lasers. Many more exciting results can be expected by further exploiting such loop couplings.

Coupling of nanowires can potentially lead to complex networks for nanophotonic systems. Law *et al*. (2004) and Sirbuly *et al*. (2005b) studied the coupling of different nanowires and nanobelts. It was interesting to see that many crystal materials that are brittle in their bulk form are remarkably strong and elastic to allow repeatedly bending, looping, and other manipulations using micro- or nanomanipulators. Complex and efficient coupling between nanowire waveguides and nanowire lasers, between different waveguides, and between waveguides and detectors can be realized using such nanoscale manipulations. Even simple optical logical circuits can be realized using crossbar nanowire network (Sirbuly *et al*., 2005a,b). Even though such coupled nanowire network can realize many complex nanophotonic functionalities and can be potentially important to achieve nanophotonic integrated systems, a more efficient and high-throughput strategy is needed to precisely control and repeatedly assemble such systems on a large scale. Such nanoscale assembly would provide an interesting alternative to the current top-down microfabrication.

9. ELECTRICAL INJECTION LASING

Electrical injection is such an important part of any semiconductor laser that it is almost automatically implied in the term ''semiconductor laser.'' Electrical injection is both a unique advantage of semiconductors compared to other lasing media and a necessity for compact applications. In order for nanowire-based lasers to realize all the promised potentials, electrical injection is indispensable, especially for applications in any nanophotonic integrated systems or on-chip systems. But electrical injection nanowire lasing has turned out to be very challenging.

Attempts to make electrical injection LEDs and lasers were made since early days of nanowire research (Duan *et al.*, 2001, 2003; Huang *et al.*, 2005). Various configurations have been experimented including cross-wire geometry, longitudinal junctions, and core–shell structures. The first report of an electrical injection nanowire lasing was made by Duan *et al.* (2003), which still represents the only one of its kind so far. The basic structure involves an n-type CdS nanowire with diameter in the range of 80–200nm and 10s–100s of microns in length, placed on a heavily p-doped Si substrate providing hole injection. After a layer of Al_2O_3 of thickness 60–80nm, top metal contact consisting of 40nm Ti and 200nm Au was placed on top of the nanowire. The device showed linewidth narrowing and nonlinear current-intensity increasing around 200μA, indicating laser threshold at room temperature. The device showed a linewidth narrowed down to 0.8nm at room temperature, comparable to similar situations under optical pumping. There are several important or intriguing features of this device. First of all, the injection geometry guaranteed that the electrical injection happens along the entire length of the nanowire, providing the long gain length and overlapping region with the propagating optical modes; both are critical for lasing. Second, the vertical structure of this device is a p–n junction, not a more standard and efficient p–i–n structure as is typical of semiconductor laser nowadays. Furthermore, the cross-section of the junction is formed by a circle tangential to a straight line, further reducing the effective volume of the junction region. Due to the band lineup between the Si and CdS, hole injection into CdS is very difficult. More likely, the electron-hole overlap happens across the interface, instead of inside the CdS nanowire. But the small junction in the vertical direction is apparently overcompensated by the long length along the wire, providing enough effective gain volume. Third, the issue of optical mode of this structure also deserves more attention. Due to the larger index of refraction of Si substrate ($\sim$3.5), CdS with an index of $\sim$2.5 would not typically be able to guide light. Optical leakage into Si would be too strong. But the overall structure has a low index middle layer consisting of CdS and Al_2O_3, sandwiched between a high-index Si and a metal layer. This is one of the typical hollow-core waveguides with gap modes guided in the lower index core. Such waveguide can be subwavelength size for certain modes. This might explain apparent good wave-guiding of the structure. Metal plasmons might have also played a role here. Finally, the mode spectrum near the threshold showed very sharp peaks as narrow as 0.3nm at room temperature at 210μA pumping, which is narrower than the linewidth of lasing mode at low temperature (0.8nm) at a much higher pumping of 280μA. It is possible that the two devices used different lengths of nanowires with the room-temperature device having a much longer wire. The long device could only be driven up to or around the threshold at room

temperature, while the short device could operate beyond its threshold at low temperature.

As indicated by this first demonstration, one of the key issues related to electrical injection lasing in nanowires is the design of a favorable injection configuration that is also compatible with the standard fabrication processes. A good design should also have large enough gain region where electrons and holes coexist. A comparative study was recently conducted (Li and Ning, 2008) to identify such a favorable scheme between a typical longitudinal p–i–n structure and a core–shell p–n junction. It was shown that the latter is much better than the former and allows higher concentration of electrons and holes to be injected. The typical carrier leakage from the minority-carrier side is not a serious issue due to the core–shell geometry. Furthermore, both type I and type II band lineups can lead to high carrier injection and the entire core can be uniformly filled by electrons and holes.

Experimentally, there have been extensive studies of both complex axial (Gudiksen *et al*., 2002) and core–shell structures (Hayden *et al*., 2005; Qian *et al*., 2004, 2005, 2008), mostly from growth point of view. Very early on, core–shell and multishell structures involving different combinations of Si and Ge were realized (Lauhon *et al*., 2002) using CVD approach with two purposes intended: to passivate the inner core materials for the enhancement of light emission and to form radial heterostructures for various device applications such as coaxially gated field-effect transistors and light-emitting devices. Recently, more complicated nitride core–shell structures were fabricated (Qian *et al*., 2004, 2005, 2008) with large numbers of quantum wells in the radial direction (Qian *et al*., 2008). Optical pumped lasing at different wavelengths using multiple GaN/InGaN quantum wells was demonstrated with different In-compositions in the well regions (Qian *et al*., 2008). Such radial multiple quantum wells can potentially form a laser structure for electrical injection lasing.

10. THEORY, MODELING, AND SIMULATION

Systematic theoretical study of semiconductor nanowires including modeling and simulation has been performed by quite a few groups including Maslov and Ning (2003, 2004a,b,c, 2005a,b, 2006, 2007a,b,c), Li and Ho (2005), Tong *et al*. (2003, 2004), Chen and Towe (2006), Zhang and Loncar (2008), and Lassen *et al*. (2006). Many aspects of these results are covered by a few extensive recent reviews (Maslov and Ning, 2007c; Ning, 2010). Here we only try to review certain aspects that are not covered there.

A complete understanding of optical and lasing properties of semiconductor nanowires involves modeling and understanding at various levels including electronic bandstructures of underlying materials with

specific nanowire or nanotube structures (Lassen *et al*., 2006; Malkova and Ning, 2007; Maslov and Ning, 2005a,b), light-emission properties of dipoles inside the nanowires (Maslov and Ning, 2006), optical modal properties (Maslov and Ning, 2003, 2004a,b,c), and lasing properties (Maslov and Ning 2004b, 2007c; Zimmler *et al*., 2010).

From the band structure point of view, some of the interesting phenomena appear only for wires with a diameter smaller than 10nm when quantum-size effects are important. For example, the issue of polarization anisotropy is known for nanowires, meaning that the optical processes such as absorption and emission are stronger for field polarization along rather than perpendicular to the nanowires. But it is interesting that this issue has origins both in dielectric screening, a classic macroscopic electromagnetic phenomenon, and in bandstructures for smaller wires (Maslov and Ning, 2005b; Persson and Xu, 2004; Sercel and Vahala, 1991). The band structure contribution increases with the reduction of wire diameter (Maslov and Ning 2005b). This anisotropy can increase from ∼60% at large diameter to ∼90% at smaller diameter for InP nanowires (Maslov and Ning, 2005b). For wurtzite nanowires such as GaN grown along the *c*-axis, it was shown that such anisotropy can be huge for a longitudinally polarized field, contrary to the bulk material of GaN (Maslov and Ning, 2005a). Another interesting consequence for the thin GaN nanowires is the existence of the dark states for nanowires as small as 3.5nm due to the band-mixing at zone center. Polarization anisotropy has important consequences on the optically pumped lasing study, since lasing threshold should depend on the polarization direction of the pumping and emitted light relative to the nanowire axis.

Light emission from dipoles inside a nanowire is an interesting topic from many perspectives and was systematically studied recently (Maslov and Ning, 2006, 2007c). From a nanolaser point of view, it is important to understand how emitted light is distributed between various modes of the cavity formed by a nanowire and the unguided modes or free-space modes, modes that propagate to the outside of nanowires. This issue is directly related to the so-called spontaneous emission, or β-factor, which describes the percentage of emission into a guided (or lasing) mode out of the total emission. When the finite size of the nanowire is treated properly, such consideration also includes the Purcell effect described by the Purcell factor, which describes the enhancement due to the restricted dielectric environment compared to dipole emission in an infinitely large (unbounded) environment. In the context of LEDs, such study provides information about extraction efficiency directly. Several interesting results (Maslov and Ning, 2006) are worth mentioning here. For example, the emission of a dipole into a given mode depends sensitively on the orientation of the dipole and on the radial location of the dipole. A purely *z*-oriented dipole placed at the center of the nanowire does not

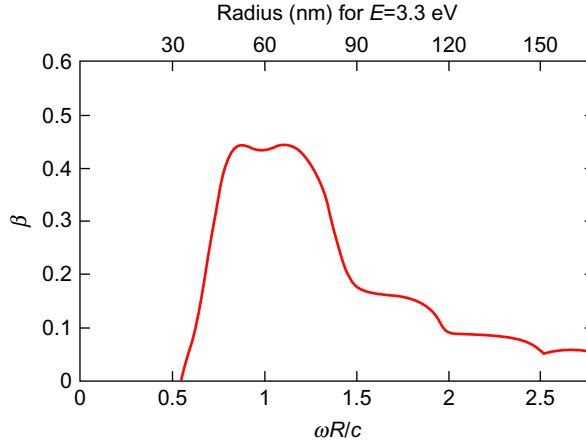

FIGURE 12.4 Spontaneous emission factor for the HE_{11} mode as a function of normalized wire radius or photon frequency.

emit into the lowest order-guided mode (HE_{11} and HE_{-11}). Such strong dependence on dipole orientation relative to the wire axis should have important consequences for designing a nanowire laser or LED using a given material of a specific growth direction. Figure 12.4 shows the spontaneous emission factor for HE_{11} mode as a function of photon frequency or wire radius (Maslov and Ning, 2006, 2007c) with a refractive index of 2.45. The maximum β-value is over 40% around normalized frequency of 1. This large value should be compared with the typical value of several thousandths in a conventional semiconductor laser. Even though the HE_{11} mode does not have a cutoff, the emission into that mode is negligible when $R<\omega/c$. For higher photon energy and or larger wires, the decrease of the β-factor is due to the appearances of other modes. Similarly, the extraction factors can also be obtained using similar simulation. Figure 12.5 shows the extraction (free-space) efficiency that is defined as the ratio of the power emitted into free-space modes to that of guided modes for various dipole components (a) and for averaged dipole (b) assuming random orientations. Consistent with the β-factor value of Fig. 12.4, the extraction efficiency is 100% for wire radius $R<\omega/c$. Due to the appearances and cutoffs of various modes, the extraction efficiencies show highly oscillatory behavior. But the z-oriented dipoles have much higher extraction efficiency than those of other dipole orientations. Even for large diameter wires, the extraction efficiency of z-orientation dipoles can be as high as 80%, despite large difference of refractive indices between the wire (2.45) and air. The extraction efficiency for nanowires is in general between 40% and 60% for random orientations

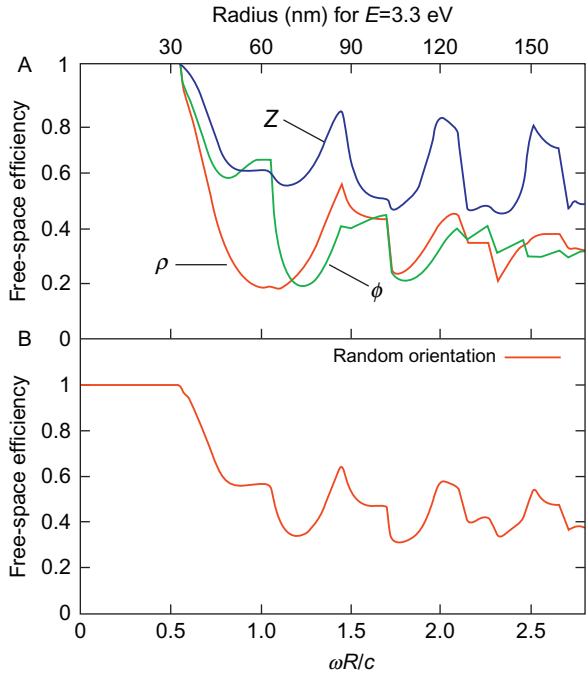

FIGURE 12.5 Extraction (freespace) efficiency defined as percentage of emission into free-space modes out of the total emission power for various dipole orientations (A) and for dipoles with random orientations (B) after averaging.

of transition dipoles. All these properties have important consequences in the design and development of nanowire-based lasers or LEDs.

Semiconductor nanowire structures such as p–n junctions and other heterostructures are also interesting from the pure dielectric screening point of view and were subjects of quite a few theoretical and simulation studies (Hu *et al.*, 2007, 2008, 2009; Leonard and Talin, 2006; Leonard and Tersoff, 1999; Ruda and Shik, 1998). Due to the finite and small cross-section of a p–n junction or a semiconductor–metal junction in a typical nanowire, the resulting imperfect screening leads to increased depletion length (Leonard and Tersoff, 1999) and increased contact resistivity (Hu *et al.*, 2008) and other behaviors (Hu *et al.*, 2007, 2009) that are significantly different from the typical bulk junctions or contacts. It was shown that the specific geometries of contacts are significant (Ruda and Shik, 1998). Such fringe-field effects become more severe when the diameters of nanowires or junctions become small. These effects will affect the design and operation of electrical injection lasers and deserve more attention in the design

of semiconductor nanowire lasers. More experimental studies are needed to compare these theoretical results with experiments.

11. SIZE REDUCTION AND METAL–DIELECTRIC CORE–SHELL STRUCTURES

Individual nanowires already represent one of the smallest lasers among all the other microlasers and nanolasers. It is always tempting to ask questions such as how small these nanowire lasers can ultimately be. Even though there is no cutoff size or wavelength for the HE_{11} mode in a cylindrical nanowire (Maslov and Ning, 2003), the modal confinement becomes too poor when the radius becomes too small (Maslov and Ning, 2003; Tong *et al*., 2004). This is why many semiconductor nanowires fail to lase for small diameters, as shown by a threshold map for various wire diameters and lengths (Zimmler *et al*., 2010).

To improve the modal confinement and to possibly further reduce sizes of nanowires to make ultra-small nanolasers, it was clear that pure dielectric waveguides are not capable of effectively guiding laser modes. This issue is also related to answering the question what the ultimate size of a nanolaser is or if there is such a size limit, as was more extensively discussed recently (Ning, 2010). It was first proposed (Maslov and Ning, 2007a,b) that a metal shell coated outside of a semiconductor core can serve as an effective waveguide. Even though a metallic-cavity surface-emitting laser was explored for enhanced spontaneous emission very early on (Yamamoto *et al*., 1991) and metallic cavity was used successfully for long wavelength lasers (Sirtori *et al*., 1998), it was thought impossible to use metallic cavities in near infrared and shorter wavelengths due to much increased metal loss. To significantly reduce the sizes of semiconductor lasers in more than one dimension beyond what is possible with dielectric lasers, a semiconductor–metal core–shell structure was proposed and systematically analyzed with plasmonic resonant behavior included (Maslov and Ning, 2007a,b). It was demonstrated by a detailed study taking into account the full plasmonic dispersion that the net modal gain can overcome the metal loss. Any remaining doubt about metallic structures quickly disappeared when the first experimental demonstration of lasing in near infrared by (Hill *et al*., 2007) was achieved. Since then, experimental and theoretical studies of metallic-cavity nanolasers have flourished (Ding *et al*., 2010, 2011a,b,c; Hill, 2010; Hill *et al*., 2007, 2009; Li and Ning, 2009, 2010; Lu *et al*., 2010; Nezhad *et al*., 2010; Noginov *et al*., 2009; Oulton *et al*., 2009; Yu *et al*., 2010) and attracted a great deal of interest and attention (Pile, 2011; Service, 2010). In a sense, the year 2007 was a historical dividing line. Before that all the micro- and nanolasers used pure dielectric cavities, while afterwards, almost all nanolasers use

metallic structures as essential wave-confinement mechanisms. Currently, metallic-cavity lasers with subwavelength sizes are mostly limited to optical pumping (Nezhad *et al*., 2010; Noginov *et al*., 2009; Oulton *et al*., 2009; Yu *et al*., 2010). For any practical applications, it is important to have such lasers operate under continuous wave (CW) electrical injection at room temperature. Progress along this line has been very rapid in a short period of 5 years. The first room-temperature subwavelength laser was demonstrated under pulse electrical injection in 2009 (Hill *et al*., 2009). One of the remarkable features of these nanolasers was that their optical thickness can be smaller than half of the wavelength (Hill *et al*., 2009). Soon nanolasers operating at 260 K was reported (Ding *et al*., 2010, 2011a,b), with the first room-temperature operation followed quickly (Ding *et al*., 2011c). The semiconductor-core metal-shell structures have become the canonical form for metallic nanolasers and served as an indispensable vehicle for the miniaturization of nanolasers and have attracted an increasing amount of attention. The combination of semiconductor nanowires and nanopillars with metallic structures turned out to be extremely fertile ground for nanophotonics.

12. CONCLUDING REMARKS AND OUTLOOK

This year marks 10th anniversary of the demonstration of the first nanowire lasers (Huang *et al*., 2001). Tremendous progress has been made in various aspects of nanowire lasers, most importantly in material growth and characterization, in understanding the basic physics processes, and in the demonstration of optically pumped lasing. As is true for any semiconductor lasers, electrical injection is indispensable in order for nanowire lasers to have any impact on real-world applications. Design, optimization, and fabrication of the most efficient electrical injection laser structures are critical to the next stage of development of nanowire lasers. Nanowire lasers ultimately have to be fabricated using high-yield mass-production processes, thus a fabrication strategy compatible with the standard laser fabrication processing is important. Nanowire lasers have not been extensively characterized in terms of their internal and external quantum efficiency, output power, beam quality, thermal properties, and reliability, even under current optical pumping conditions. Another interesting area is high-power applications using large array of nanowires with optimized wire distribution in the array to optimize far-field output. Finally, one of the intrinsic advantages of nanowire lasers is the small size, important for eventual nanophotonic integrated systems (Yang *et al*., 2010). Thus integrating nanowire lasers with other optoelectronic devices such as detectors, waveguides, and modulators should be seriously considered and researched. For all these future efforts, more

involvement of optoelectronics device physicists and engineers are important. Great challenges and opportunities remain for material scientists, device physicists and engineers, and nanotechnologists in general.

ACKNOWLEDGMENTS

Various research projects covered in this review were supported by NASA, several NASA Ames Director's Discretionary Fund Grants, Science Foundation of Arizona, Army Research Office (Award No: W911NF-08-1-0471). I thank many government program managers for their support of my nanowire research over the past 10 or so years, including Meyya Meyyappan, Harry Partridge, and Mike Gerhold. The author thanks many of his former and current students and postdocs including Debin Li, Ruibin Liu, Alex Maslov, Patricia Nichols, Anlian Pan, Minghua Sun, and Sreeram Vaddiraju. I would also like to thank Peidong Yang for the discussions and collaborations over the past several years.

REFERENCES

Agarwal, R., Barrelet, C. J., and Lieber, C. M. (2005). *Nano Lett.* **5,** 917.
Bierman, M. J., Lau, Y. K. A., and Jin, S. (2007). *Nano Lett.* **7,** 2907.
Chen, L., and Towe, E. (2006). *Appl. Phys. Lett.* **89,** 053125.
Chen, R., Tran, T.-T. D., Ng, K. W., Ko, W. S., Chuang, L. C., Sedgwick, F. G., and Chang-Hasnain, C. (2011). *Nat. Photonics* **5,** 170.
Chin, A., Vaddiraju, S., Maslov, A. V., Ning, C. Z., Sunkara, M., and Meyyappan, M. (2006). *Appl. Phys. Lett.* **88,** 163115.
Das, A., Heo, J., Jankowski, M., Guo, W., Zhang, L., Deng, H., and Bhattacharya, P. (2011). *Phys. Rev. Lett.* **107,** 066405.
Ding, K., Liu, Z., Yin, L., Hill, M. T., Marell, J. H., van Veldhoven, P. J., Noetzel, R., and Ning, C. Z. (2010). IEEE Photonics Society Annual Meeting, Post deadline paper Nov, Denver, CO.
Ding, D., Liu, Z., Yin, L., Hill, M. T., Marell, M. J., van Veldhoven, P. J., Nötzel, R., and Ning, C. Z. (2011a). IEEE Photonics Society Winter Topical Meetings, paper TuA2.4, 10–12, Jan, 2011, Keystone, CO.
Ding, D., Liu, Z., Yin, L., Hill, M. T., Marell, M. J., van Veldhoven, P. J., Nötzel, R., and Ning, C. Z. (2011b). CLEO 2011, paper CTuG2 (May 3), Conference Program, p 100, Baltimore, MD.
Ding, D., Liu, Z., Yin, L., Wang, H., Liu, R., Hill, M. T., Marell, M. J., van Veldhoven, P. J., Nötzel, R., and Ning, C. Z. (2011c). *Appl. Phys. Lett.* **98,** 231108.
Ding, J. X., Zapien, J. A., Chen, W., Meng, X. M., Lifshitz, Y., and Lee, S. T. (2004). *Appl. Phys. Lett.* **85,** 2361.
Duan, X. F., Huang, Y., Agarwal, R., and Lieber, C. M. (2003). *Nature* **421,** 241–245.
Duan, X., Huang, Y., Cui, Y., Wang, J., and Lieber, C. M. (2001). *Nature* **409,** 66.
Duan, X. F., and Lieber, C. M. (2000). *Adv. Mater.* **12,** 298–302.
Fan, H. J., Werner, P., and Zacharias, M. (2006). *Small* **2,** 700.
Finkelman, R. B., Larson, R. R., and Dwornik, E. J. (1974). *J. Cryst. Growth* **22,** 159.
Gao, Q., Tan, H. H., Jackson, H. E., Smith, L. M., Yarrison-Rice, J. M., Zou, J., and Jagadish, C. (2011). *Semicond. Sci. Technol.* **26,** 014035.
Gargas, D., Toimil-Molares, M. E., and Yang, P. D. (2009). *J. Am. Chem. Soc.* **131,** 2125.
Gudiksen, M. S., Lauhon, L. J., Wang, J. F., Smith, D. C., and Lieber, C. M. (2002). *Nature* **415,** 617.

Haraguchi, K., Katsuyama, T., Hiruma, K., and Ogawa, K. (1992). *Appl. Phys. Lett.* **60,** 745.
Hayden, O., Greytack, A. B., and Bell, D. C. (2005). *Adv. Mater.* **17,** 701.
Heo, J., Guo, W., and Bhattacharya, P. (2011). *Appl. Phys. Lett.* **98,** 021110.
Hill, M. T. (2010). *J. Opt. Soc. Am.* **B27,** B36.
Hill, M. T., Marell, M., Leong, E. S. P., Smalbrugge, B., Zhu, Y., Sun, M. H., Vanveldhoven, P. J., Geluk, E. J., Karouta, F., Oei, Y. S., *et al*. (2009). *Opt. Express.* **17,** 11107.
Hill, M. T., Oei, Y.-S., Smalbrugge, B., Zhu, Y., de Vries, T., van Veldhoven, P. J., van Otten, F. W., Eijkemans, T. J., Turkiewicz, J. P., de Waardt, H., *et al.* (2007). *Nat. Photonics* **1,** 589.
Hu, J., Liu, Y., Maslov, A. V., Ning, C. Z., Dutton, R., and Kang, S. M. (2007). Proceedings of SPIE, p. 64681E, Vol. 6468.
Hu, J., Liu, Y., Ning, C. Z., Dutton, R., and Kang, S. M. (2008). *Appl. Phys. Lett.* **92,** 083503.
Hu, J., Liu, Y., Ning, C. Z., Dutton, R., and Kang, S. M. (2009). Proceedings of SPIE, p. 72110Q, Vol. 7211.
Hu, J., Odom, T. W., and Lieber, C. M. (1999). *Acc. Chem. Res.* **32,** 435.
Hua, B., Motohisa, J., Kobayashi, Y., Hara, S., and Fukui, T. (2009). *Nano Lett.* **9,** 112.
Huang, Y., Duan, X., and Lieber, C. M. (2005). *Small* **1,** 142.
Huang, M. H., Mao, S., Feick, H., Yan, H., Wu, Y., Kind, H., Weber, E., Russo, R., and Yang, P. D. (2001). *Science* **292,** 1897.
Huang, K., Yang, S., and Tong, L. (2007). *Appl. Opt.* **46,** 1429.
Jagadish, C., Thelander, K. D., LaPierre, R., and Motohisa, J. (2011). *IEEE J. Sel. Top. Quantum Electron.* **17,** 766.
Johnson, J., Choi, H. J., Knutsen, K. P., Schaller, R., Yang, P. D., and Saykally, R. (2002). *Nat. Mater.* **1,** 106.
Johnson, J., Yan, H., Schaller, R., Haber, L., Saykally, R., and Yang, P. D. (2001). *J. Phys. Chem.* **B105,** 11387.
Joyce, H. J., Gao, Q., Wong-Leung, J., Kim, Y., Tan, H. H., and Jagadish, C. (2011). *IEEE J. Sel. Top. Quantum Electron.* **17,** 766.
Kuykendall, T., Ulrich, P., Aloni, S., and Yang, P. D. (2007). *Nat. Mater.* **6,** 951.
Lassen, B., Willatzen, M., Melnik, R., and Lew Yan Voon, L. C. (2006). *J. Mater. Res.* **21,** 2927.
Lauhon, L. J., Gudiksen, M. S., and Lieber, C. M. (2004). *Philos. Trans. R. Soc. Lond. A* **362,** 1247.
Lauhon, L. J., Gudiksen, M. S., Wang, D., and Lieber, C. M. (2002). *Nature* **420,** 57.
Law, M., Sirbuly, D. J., Johnson, J. C., Goldberger, J., Saykally, R. J., and Yang, P. D. (2004). *Science* **305,** 1269.
Leonard, F., and Talin, A. (2006). *Phys. Rev. Lett.* **97,** 026804.
Leonard, F., and Tersoff, J. (1999). *Phys. Rev. Lett.* **83,** 5174.
Li, Z. Y., and Ho, K. M. (2005). *Phys. Rev.* **B71,** 045315.
Li, G., Jiang, Y., Wang, Y., Wang, C., Sheng, Y., Jie, J., Zapien, J. A., Zhang, W. J., and Lee, S. T. (2009). *J. Phys. Chem.* **C113,** 17183.
Li, D. B., and Ning, C. Z. (2008). *Nano Lett.* **8,** 4234.
Li, D. B., and Ning, C. Z. (2009). *Phys. Rev.* **B80,** 153304.
Li, D. B., and Ning, C. Z. (2010). *Appl. Phys. Lett.* **96,** 181109.
Liu, Y. K., Zapien, J. A., Shan, Y. Y., Geng, C. Y., Lee, C. S., and Lee, S. T. (2005). *Adv. Mater.* **17,** 1372.
Liu, Y. K., Zapien, J. A., Shan, Y. Y., Tang, H., Lee, C. S., and Lee, S. T. (2007). *Nanotechnology* **18,** 365606.
Lu, C., Chang, S., Chuang, S. C., Germann, T. D., and Bimberg, D. (2010). *Appl. Phys. Lett.* **96,** 251101.
Malkova, N., and Ning, C. Z. (2007). *Phys. Rev. B* **75,** 155407.
Maslov, A. V., and Ning, C. Z. (2003). *Appl. Phys. Lett.* **83,** 1237.
Maslov, A. V., and Ning, C. Z. (2004a). *Opt. Lett.* **29,** 572.
Maslov, A. V., and Ning, C. Z. (2004b). *IEEE J. Quantum Electron.* **40,** 1389.

Maslov, A. V., and Ning, C. Z. (2004c). *In* ''Physics and Simulation of Optoelectronic Devices XII,'' (M. Osinski, H. Amano, and F. Henneberger, eds.), Proceedings of SPIE (SPIE, Bellingham, WA), p. 24, Vol. 5349.
Maslov, A. V., and Ning, C. Z. (2005a). *Phys. Rev.* **B72,** 125319.
Maslov, A. V., and Ning, C. Z. (2005b). *Phys. Rev. B* **72,** 161310 (rapid communication).
Maslov, A. V., and Ning, C. Z. (2006). *J. Appl. Phys.* **99,** 024314.
Maslov, A. V., and Ning, C. Z. (2007a). Conference on Lasers and Electro-Optics, paper JWA 121, Baltimore, Maryland, May 6, 2007.
Maslov, A. V., and Ning, C. Z. (2007b). *In* ''Physics and Simulation of Optoelectronic Devices XV,'' (M. Osinski, F. Henneberger, and Y. Arakawa, eds.), Proceedings of SPIE, (SPIE, Bellingham, WA), p. 64680I, Vol. 6468.
Maslov, A. V., and Ning, C. Z. (2007c). *In* ''Nitride Semiconductor Devices: Principles and Simulation,'' (J. Piprek, ed.). Wiley-VCH GmbH and Co, Weinheim.
Moore, D., and Wang, Z. L. (2006). *J. Mater. Chem.* **16,** 3898.
Nezhad, M., Simic, A., Bondarenko, O., Slutsky, B., Mizrahi, A., Feng, L., Lomakin, V., and Fainman, Y. (2010). *Nat. Phontonics* **4,** 395.
Nichols, P. L., Sun, M. H., and Ning, C. Z. (2011). *ACS Nano* **5,** 8730–8738. doi: 10.1021/nn202704u.
Ning, C. Z. (2010). *Physica Status Solidi* **B247,** 774.
Noginov, M. A., Zhu, G., Belgrave, A. M., Bakker, R., Shalaev, V. M., Narimanov, E. E., Stout, S., Herz, E., Suteewong, T., and Wiesner, U. (2009). *Nature* **460,** 1110.
Oulton, R. F., Sorger, V. J., Zentgraf, T., Ma, R. M., Gladden, C., Dai, L., Bartal, G., and Zhang, X. (2009). *Nature* **461,** 629.
Pan, A., Liu, R. B., Sun, M. H., and Ning, C. Z. (2009a). *J. Am. Chem. Soc.* **131,** 9502.
Pan, A., Liu, R., Sun, M. H., and Ning, C. Z. (2010). *ACS Nano* **4**(2), 671–680.
Pan, A., Liu, R., Wang, F., Xie, S., Zou, B. S., Zacharias, M., and Wang, Z. L. (2006). *J. Phys. Chem. B* **110,** 22313–22317.
Pan, A., Nichols, P. L., and Ning, C. Z. (2011). *IEEE J. Sel. Top. Quantum Electron.* **17,** 808.
Pan, A. L., Yang, H., Liu, R., Yu, R., Zou, B., and Wang, Z. L. (2005). *J. Am. Chem. Soc.* **127,** 15692.
Pan, A., Zhou, W., Leong, E. S. P., Liu, R., Chin, A. H., Zou, B., and Ning, C. Z. (2009b). *Nano Lett.* **9,** 784.
Pauzauskie, P., Sirbuly, D., and Yang, P. D. (2006). *Phys. Rev. Lett.* **96,** 143903.
Pauzauskie, P. L., and Yang, P. D. (2006). *Mater. Today* **9,** 36.
Persson, M. P., and Xu, H. Q. (2004). *Phys. Rev. B* **70,** 161310 (R).
Pile, D. (2011). *Nat. Photonics* **5,** 12.
Qian, F., Gradecak, S., Li, Y., Wen, C. Y., and Lieber, C. M. (2005). *Nano Lett.* **5,** 2287.
Qian, F., Li, Y., Gradecak, S., Barrelet, C. J., Wang, D., and Lieber, C. M. (2004). *Nano Lett.* **4,** 1975.
Qian, F., Li, Y., Gradecak, S., Park, H., Dong, Y., Ding, Y., Wang, Z. L., and Lieber, C. M. (2008). *Nat. Mater.* **7,** 701.
Ruda, H., and Shik, A. (1998). *J. Appl. Phys.* **84,** 5867.
Samuelson, L. (2003). *Mater. Today* **6,** 22.
Sercel, P. C., and Vahala, K. J. (1991). *Phys. Rev. B* **44,** 5681.
Service, R. (2010). *Science* **328,** 810.
Shirai, M., Haraguchi, K., Hiruma, K., and Katsuyama, T. (1999). *Gold Bull.* **32,** 80.
Sirbuly, D., Law, M., Pauzauskie, P., Yan, H., Maslov, A., Knutzen, K., Ning, C. Z., Saykally, R., and Yang, P. D. (2005a). *Proc. Natl. Acad. Sci. USA* **102,** 7800.
Sirbuly, D., Law, M., Yan, H., and Yang, P. D. (2005b). *J. Phys. Chem. B* **109,** 15191 (feature article).
Sirtori, C., Gmachl, C., Capasso, F., Faist, J., Sico, D. L., Hutchinson, A. L., and Cho, A. Y. (1998). *Opt. Lett.* **23,** 1366.

Sun, M. H., Nichols, P. L., and Ning, C. Z. (2011) (to be published).
Thelander, C., Agarwal, P., Brongersma, S., Eymery, J., Feiner, L. F., Forchel, A., Scheffler, M., Riess, M., Ohlsson, B. J., Gösele, U., *et al.* (2006). *Mater. Today* **9,** 28.
Tomioka, K., Tanaka, T., Hara, S., Hiruma, K., and Fukui, T. (2011). *IEEE J. Sel. Top. Quantum Electron.* **17,** 1112.
Tong, L. M., Gattass, R. R., Ashcom, J. B., He, S., Lou, J., Shen, M., Maxwell, I., and Mazur, E. (2003). *Nature* **426,** 816.
Tong, L. M., Lou, J., and Mazur, E. (2004). *Opt. Express* **12,** 1025.
Vaddiraju, S., Chin, A., Maslov, A. V., Ning, C. Z., Sunkara, M., and Meyyappan, M. (2007). *J. Phys. Chem.* **C111,** 7339.
Vanmaekelbergh, D., and van Vugt, L. K. (2011). *Nanoscale* **3,** 2783.
Wagner, R. S., and Ellis, W. C. (1964). *Appl. Phys. Lett.* **4,** 89.
Wang, Z. L. (2009). *Mater. Sci. Eng.* **R64,** 33.
Wang, H., Sun, M. H., Ding, K., Hill, M. T., and Ning, C. Z. (2011). *Nano Lett.* **11,** 1646.
Wu, Y. Y., and Yang, P. D. (2001). *J. Am. Chem. Soc.* **123,** 3165–3166.
Xiao, Y., Meng, C., Wang, P., Ye, Y., Yu, H., Wang, S., Gu, F., Dai, L., and Tong, L. (2011a). *Nano Lett.* **11,** 1122.
Xiao, Y., Meng, C., Wu, X., and Tong, L. (2011b). *Appl. Phys. Lett.* **99,** 023109.
Yamamoto, Y., Machida, S., and Bjork, G. (1991). *Phys. Rev.* **A44,** 657.
Yan, R., Gargas, D., and Yang, P. D. (2009). *Nat. Photonics* **3,** 569.
Yan, H., He, R., Johnson, J., Law, M., Saykally, R. J., and Yang, P. D. (2003a). *J. Am. Chem. Soc.* **125,** 4728.
Yan, H., Justin, J., Law, M., Saykally, R. J., and Yang, P. D. (2003b). *Adv. Mater.* **15,** 1907.
Yang, P. D. (2002). *In* Global Photonics Applications and Technology World Markets Series pp. 42–47. Business Briefing.
Yang, P. D., Fardy, M., and Yan, R. (2010). *Nano Lett.* **10,** 1529.
Yang, P. D., Yan, H., Mao, S., Russo, R., Johnson, J., Saykally, R. J., Morris, N., Pham, J., He, R., and Choi, H. (2002). *Adv. Funct. Mater.* **12,** 323 (invited feature article).
Yazawa, M., Koguchi, M., and Hiruma, K. (1991). *Appl. Phys. Lett.* **58,** 1080.
Yu, K., Lakhani, A., and Wu, M. (2010). *Opt. Express* **18**(9), 8790–8799.
Zapien, J. A., Jiang, Y., Meng, X. M., Chen, W., Au, F. C. K., Lifshitz, Y., and Lee, S. T. (2004). *Appl. Phys. Lett.* **84,** 1189.
Zapien, J. A., Liu, Y. K., Shan, Y. Y., Tang, H., Lee, C. S., and Lee, S. T. (2007). *Appl. Phys. Lett.* **90,** 213114.
Zhang, Y., and Loncar, M. (2008). *Opt. Express* **16,** 17400.
Zimmler, M. A., Bao, J., Capasso, F., Muller, S., and Ronning, C. (2008). *Appl. Phys. Lett.* **93,** 051101.
Zimmler, M. A., Capasso, F., Muller, S., and Ronning, C. (2010). *Semicond. Sci. Technol.* **25,** 024001.